Chemical Science

ROYAL SOCIETY OF CHEMISTRY

EDGE ARTICLE

View Article Online
View Journal | View Issue

Cite this: *Chem. Sci.*, 2025, **16**, 17214

All publication charges for this article have been paid for by the Royal Society of Chemistry

Received 7th July 2025
Accepted 19th August 2025

DOI: 10.1039/d5sc05042a

rsc.li/chemical-science

Solvent-dependent reactivity of azo-BF_2 switches

Qingkai Qi,†[ab] Heyifei Fu,†[a] Lingya Peng,†[c] Shefali Patra,[a] Xiaogang Liu[c] and Ivan Aprahamian*[a]

Azo-BF_2 complexes are visible and near-infrared (NIR) light-activated photoswitches showcasing versatility in applications ranging from energy storage to three-dimensional displays. While highly appealing as molecular switches, factors that affect their photophysical properties and solution-state reactivity still need to be teased out. In this paper, we present the synthesis and characterization of two azo-BF_2 analogues (**1** and **2**), each modified with structurally distinct dimethylamine-substituted naphthalene moieties. In addition to investigating the effect of the π-system expansion on the photophysical and photoswitching properties of the system, we also elaborate on the stability (*i.e.*, whether they undergo solvolysis or 1,2-BF_2 shift) of the switches in different solvents. Specifically, switch **1** absorbs in the NIR region, enabling its activation with 700 nm light, while switch **2** exhibits enhanced separation between the *trans* and *cis* isomer absorption bands, resulting in an improved photostationary state. As for the solvent effect, we discovered that polar aprotic solvents induce an intramolecular 1,2-BF_2 shift in both switches, transforming the azo-BF_2 photoswitches into boron difluoride hydrazone fluorophores, whereas polar protic solvents facilitate the solvolysis of the azo-BF_2 into the starting hydrazone derivative. In the former, the donor number of the solvent is a major factor in determining the obtained outcome, while in the latter, it is the solvent's hydrogen-bond donation capability. These insights into the design strategy and solvent-mediated reactivity of azo-BF_2s will contribute to their further development into efficient NIR-responsive photoswitches, paving the way for innovative applications in smart materials and molecular devices.

Introduction

Visible and near-infrared (NIR) light-activated photoswitches have gained popularity in the fields of photopharmacology and adaptive materials in recent years,[1–8] because they enable deep substrate penetration while maintaining low phototoxicity. This interest resulted in the development of an array of red-light and NIR-activated photoswitches, such as azobenzenes,[9–17] diarylethenes,[18–21] indigoids,[22–25] dihydropyrenes,[26,27] donor–acceptor Stenhouse adducts,[28–32] and heteroaryl azoswitches.[33,34] Our contribution to this research area was the introduction of azo-BF_2 photoswitches,[35] which were the first azobenzene derivatives to be activated with NIR light.[36] These switches also exhibit other sought-after characteristics, such as high photostationary states (PSS), enhanced isomerization quantum yields (Φ), and negative photochromism. We recently took advantage of these unique features to develop a rewritable, solid-state, hand-held volumetric 3D photochromic display capable of showcasing both static 3D images and dynamic 2D animations.[37] We also demonstrated how such photoswitches can be used in molecular solar thermal energy storage applications.[38] Beyond these applications, structural modifications of azo-BF_2 switches have revealed several key insights: (1) extending the π-system from quinolinyl to phenanthridinyl results in self-aggregates that enhance the half-life ($\tau_{1/2}$) of its thermal relaxation;[39] (2) an oxygen atom adjacent to the BF_2 bridge can induce a thermal 1,2-BF_2 shift, converting the azo-BF_2 photoswitch into a borondifluorohydrazone (BODIHY) in both solution and the solid state;[40] and (3) increasing the electron density through *para*-substitution causes a bathochromic shift in the activation wavelength, enabling control over the *trans*/*cis* isomerization process using NIR light.[36] Nonetheless, and despite the many promising features of azo-BF_2 switches, practical applications in the solution state are hindered by their reactivity, especially in polar media, particularly water. Hence, understanding the solvent interactions with these switches is an essential step towards extending their utility, especially *in vivo* settings.

Here, we report on two azo-BF_2 analogues (**1** and **2**) that incorporate an *N*,*N*-dimethylnaphthalen-1-amine or *N*,*N*-dimethylnaphthalen-2-amine moiety attached at the 5 or 6-

[a]*Department of Chemistry, Dartmouth College, Hanover, New Hampshire 03755, USA. E-mail: ivan.aprahamian@dartmouth.edu*

[b]*Jiangsu Collaborative Innovation Center of Biomedical Functional Materials, School of Chemistry and Materials Science, Nanjing Normal University, Nanjing 210023, China*

[c]*Fluorescence Research Group, Singapore University of Technology and Design, Singapore*

† These three authors contributed equally.

position, respectively (Fig. 1a). Our initial goal was to investigate how modifications to the π-system will influence the activation wavelength and overall photoswitching efficiency compared to the parent azo-BF_2. Structural analysis revealed that these two switches exhibit distinct photophysical properties and photoswitching performances. Specifically, the absorption spectrum of **1** extends into the NIR region, thus allowing NIR activation. In contrast, switch **2** has a more pronounced separation between the *trans* and *cis* absorption bands, resulting in an improved PSS ratio.

To gain a deeper understanding of how polar solvent environments affect the molecular properties of the switches, we systematically examined the behavior of both derivatives under various solvent environments. Our focus was on understanding the correlation between their stability and key solvent parameters, including donor number (DN), dipolarity/polarizability (π*), basicity, and hydrogen bond donation ability (α).[41] We discovered that polar aprotic solvents such as dimethyl sulfoxide (DMSO), dimethylformamide (DMF), and dimethylacetamide (DMAc) induce the intramolecular 1,2-BF_2 shift in both derivatives, leading to the formation of the BODIHY product (Fig. 1b and c). In solvents such as acetone, tetrahydrofuran (THF), ethyl acetate (EA) and polar protic alcohols both switches undergo solvolysis yielding their starting hydrazones, though at different time-scales. A comprehensive analysis of solvent parameters revealed a strong correlation between the DN of the solvents and the rate of BODIHY formation, suggesting that solvents with a greater lone pair donation ability result in a more efficient 1,2-BF_2 shift. In solvents with lower DN (*e.g.*, acetone, THF, and EA), both switches undergo solvolysis, regenerating their original hydrazones on a timescale comparable to that of the BF_2 shift. We hypothesize that the trace amounts of water (<50 ppm) present in these solvents facilitate solvolysis; in contrast, in non-nucleophilic solvents such as toluene and dichloromethane (DCM), no reaction is observed. On the other hand, the relatively fast solvolysis of the azo-BF_2 switches to their hydrazone precursors in polar protic alcohols is primarily driven by the solvents' hydrogen bond donation ability (α).

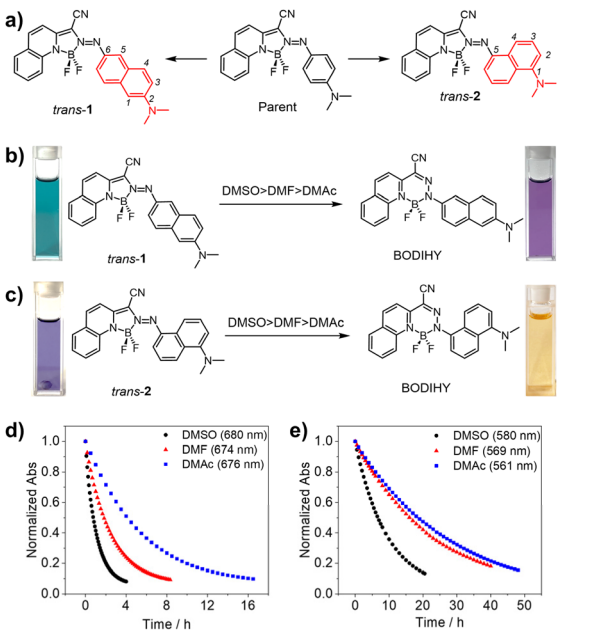

Fig. 1 (a) The structures of the two azo-BF_2 derivatives **1** and **2**. (b) Photographs of the solution of *trans*-**1** and (c) *trans*-**2** before and after the 1,2-BF_2 shift in various solvents, along with their corresponding molecular structures. (d) Kinetic profiles of the 1,2-BF_2 shift of *trans*-**1** and (e) *trans*-**2** in DMSO, DMF, and DMAc (4×10^{-5} M).

Results and discussion

Azo-BF_2s **1** and **2** were synthesized by reacting their respective hydrazone precursors with boron trifluoride diethyl etherate, in the presence of *N*,*N*-diisopropylethylamine (Schemes S1 and S2). The azo-BF_2 switches and their precursors were fully characterized using NMR spectroscopy and mass spectrometry (Fig. S1–S13).

The photoisomerization performance of the switches in DCM was evaluated using UV-Vis and NMR spectroscopies (Fig. S14–S20), and the data are summarized in Table 1. Switch **1** predominantly exists in its thermodynamically stable *trans* form in the dark (95%), with a maximum UV-Vis absorbance (λ_{max}) at 675 nm ($\varepsilon = 34\,300\ M^{-1}\ cm^{-1}$, Fig. 2c) and an absorption tail extending to approximately 800 nm. While the λ_{max} is slightly blue-shifted relative to the parent system ($\lambda_{max} = 680$ nm), the absorption tail extends further by 50 nm into the near-infrared region, making it the most red-shifted azo-BF_2 system reported to date. These results indicate that attaching a naphthyl group to the azo-BF_2 core through the β-position effectively elongates the π-conjugation. Upon irradiation with 700 nm light, the *cis* isomer ($\lambda_{max} = 620$ nm; $\varepsilon = 17\,500\ M^{-1}\ cm^{-1}$, Fig. 2c) becomes predominant, accompanied by a slight color change of the solution from greenish cyan to cyan blue (Fig. 2a). The thermal half-life ($\tau_{1/2}$) of the metastable *cis*-**1** isomer in aerated DCM was measured to be 2.2 ± 0.01 min at 294 K (Fig. S25). Because of the rapid back isomerization, accurate PSS_{700} could not be determined. The lowest estimated amount of the *cis* isomer at PSS_{700} is 47% (Fig. S16), with a quantum yield ($\Phi_{trans\rightarrow cis}$) of 13.6 ± 1.7% (Fig. S21). This value is underestimated because of the fast back isomerization process. A deduced absorption curve for *cis*-**1**, based on previously reported methods,[42,43] gives a λ_{max} of 595 nm with an ε of $15\,800\ M^{-1}\ cm^{-1}$ (Fig. 2c), yielding a $\Delta\lambda_{max}$ value of 80 nm. Further irradiation at 480 nm results in a PSS_{480} of 63% *trans* (Fig. S16) and a $\Phi_{cis\rightarrow trans}$ of 35.1 ± 2.7% (Fig. S22). This value is overestimated because of the fast back isomerization process. The relatively low PSS values for both the forward and backward photoisomerization processes are attributed to the significant overlap of the absorption bands of the two isomers and the short $\tau_{1/2}$. The photoswitching can be cycled multiple times with no signs of photodegradation (Fig. S14c).

Switch **2** exists predominantly in the *trans* form (62–64%, Fig. S53 and S54) when equilibrated under dark ($\lambda_{max} = 578$ nm, $\varepsilon = 21\,300\ M^{-1}\ cm^{-1}$, Fig. 2d). The λ_{max} of *trans*-**2** is blue shifted by around 100 nm from that of the parent compound ($\lambda_{max} =$ 680 nm) and *trans*-**1** ($\lambda_{max} = 675$ nm), as the NMe_2 group is not

Table 1 Summary of photophysical data for azo-BF_2s **1** and **2** in DCM

	λ_{abs}[a] (nm)/ε[b] ($M^{-1}cm^{-1}$)		PSS (%) @ λ_{irr}[c] (nm)		Φ_{isom} (%)[d]		
Azo-BF_2	*trans*	*cis*	*trans* : *cis*	*trans* : *cis*	*trans* → *cis*	*cis* → *trans*	$\tau_{1/2}$[e] (min)
1	675/34 300	595/15 800[f]	25 : 75 @ 700[f]	63 : 37 @ 480	13.6 ± 1.7	35.1 ± 2.7	2.2 ± 0.1
2	578/21 300	473/19 800[f]	21 : 79 @ 650[f]	67 : 33 @ 442	6.3 ± 0.1	24.7 ± 2.3	384 ± 4

[a] Absorption maximum. [b] Extinction coefficient. [c] Photostationary state measured at the optimal irradiation wavelength. [d] Photoisomerization quantum yield. [e] Thermal half-life of the *cis* → *trans* transformation at 298 K. [f] Deduced using previously reported methods.[41,42]

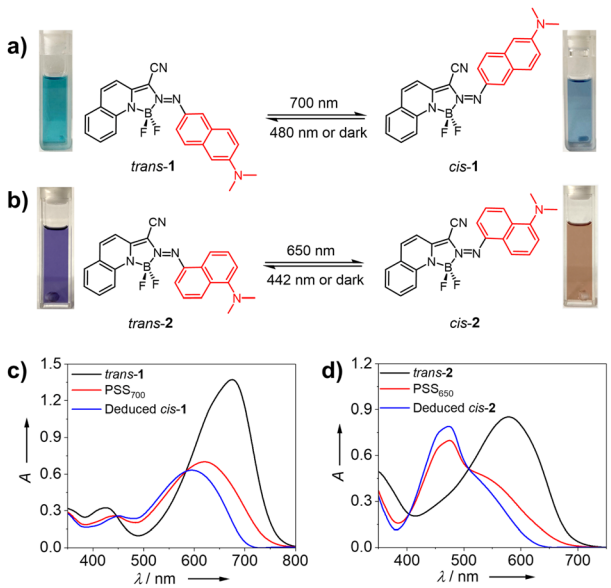

Fig. 2 Light-induced *trans*/*cis* isomerization of (a) **1** and (b) **2**, along with the corresponding UV/vis absorption changes (c) and (d), respectively, in DCM (4×10^{-5} M).

in direct conjugation with the azo core. Upon irradiation with 650 nm light, *trans*-**2** switches to its *cis* form ($\lambda_{max} = 475$ nm, $\varepsilon = 17\,500\ M^{-1}\ cm^{-1}$; deduced $\lambda_{max} = 473$ nm, $\varepsilon = 19\,800\ M^{-1}\ cm^{-1}$; Fig. 2d), accompanied by a drastic color change of the solution from purple to brown (Fig. 2b). The PSS_{650} for *trans*-**2** was measured to be 74% *cis* (Fig. S17), with a $\Phi_{trans \rightarrow cis}$ of 6.3 ± 0.1% (Fig. S23). Switch **2** exhibits a better band separation between the *trans* and *cis* isomers than switch **1** ($\Delta\lambda_{max}$: 105 *vs.* 80 nm, respectively). The reverse process (*cis* → *trans*) can be triggered using a 442 nm light source, resulting in a PSS_{442} of 67% *trans* (Fig. S17) and a $\Phi_{cis \rightarrow trans}$ of 24.7 ± 2.3% (Fig. S24). The $\tau_{1/2}$ for the *cis* → *trans* process of switch **2** was calculated to be 384 ± 4 min (Fig. S26), approximately 175 times longer than that of switch **1**. Again, and as previously discussed, this difference is attributed to the fact that the NMe_2 group is not in direct conjugation with the azo core. The longer $\tau_{1/2}$ allows for a better assessment of the system's photoswitching efficacy. The photoswitching can be cycled numerous times with no signs of photodegradation (Fig. S15c).

The major challenge with using azo-BF_2 switches in the solution state lies in the stability of the N → B coordination bond, which can undergo 1,2-BF_2 shift and/or hydrolysis. It should be noted here that this reactivity is mainly observed for the *trans* form, while the *cis* isomer is far more stable.[36,40] To probe the effect of solvent polarity and proticity on the stability of this bond, we conducted a comprehensive investigation across a range of solvents (Fig. 1d and e). Both switches exhibit good stability, *i.e.*, undergo no reaction, in non-polar solvents such as DCM (Fig. S41 and S42) and toluene (Fig. S53 and S54). On the other hand, polar aprotic solvents such as DMSO, DMF,

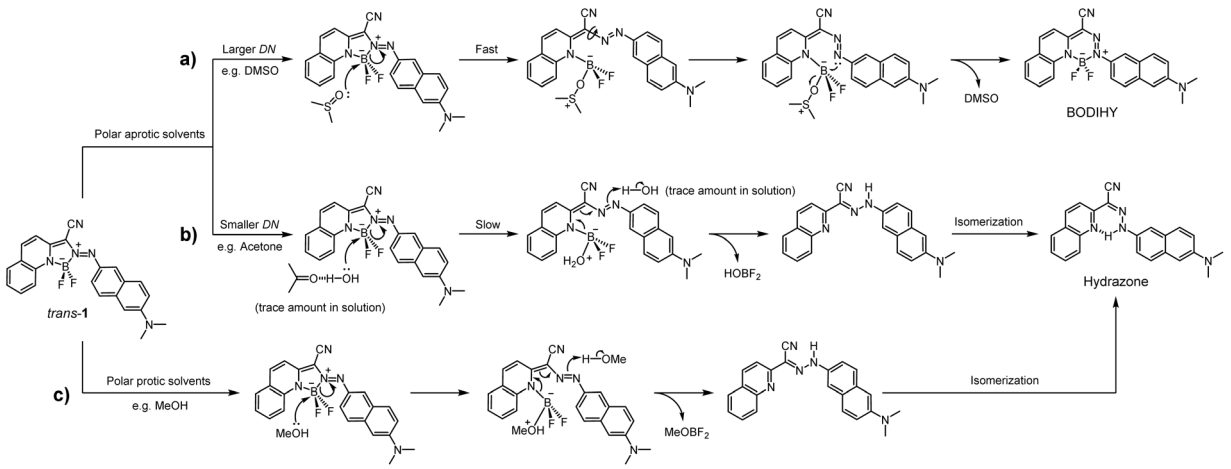

Fig. 3 Proposed reaction mechanisms for azo-BF_2 compounds. (a) 1,2-BF_2 shift in polar aprotic solvents having high DN (*e.g.*, DMSO); (b) solvent-assisted slow solvolysis in polar aprotic solvents with low DN (*e.g.*, acetone); and (c) rapid solvolysis in polar protic solvents (*e.g.*, MeOH).

Table 2 Summary of decomposition data for both azo-BF_2s in aprotic solvents

		1		**2**	
Azo-BF_2s	Donor number	$\tau_{1/2}$[a] (h)	k[b] (s^{-1})	$\tau_{1/2}$[a] (h)	k[b] (s^{-1})
DMSO[c]	29.8	0.68 ± 0.03	$2.8 \pm 0.1 \times 10^{-4}$	6.2 ± 0.6	$3.1 \pm 0.3 \times 10^{-5}$
DMF[c]	26.6	1.8 ± 0.2	$1.1 \pm 0.1 \times 10^{-4}$	16 ± 1	$1.2 \pm 0.1 \times 10^{-5}$
DMAc[c]	27.8	3.3 ± 0.4	$5.8 \pm 0.6 \times 10^{-5}$	17 ± 2	$1.1 \pm 0.1 \times 10^{-5}$
THF[d]	20.0	44 ± 3	$4.4 \pm 0.3 \times 10^{-6}$	36 ± 5	$5.5 \pm 0.8 \times 10^{-6}$
Acetone[d]	17.0	53 ± 7	$3.7 \pm 0.4 \times 10^{-6}$	109 ± 9	$1.8 \pm 0.2 \times 10^{-6}$
EA[d]	17.1	82 ± 15	$2.4 \pm 0.4 \times 10^{-6}$	184 ± 26	$1.1 \pm 0.1 \times 10^{-6}$

[a] *Trans*-**1** decomposition half-life. [b] The reaction rate of decomposition. [c] 1,2-BF_2 Shift. [d] Solvolysis.

and DMAc initiate an intramolecular 1,2-BF_2 shift in both switches, leading to the formation of BODIHY products (Fig. S35–S37 and S44–S46). We hypothesize that these polar aprotic solvents coordinate with the boron core of the azo-BF_2 switches, leading to the cleavage of the intramolecular N → B coordination bond (Fig. 3a). The resulting bond dissociation increases the rotational freedom of the C–N single bond, allowing it to adopt a conformation that favors the formation of a new and more stable intramolecular N → B bond. This transformation is reminiscent of our earlier finding, where an oxygen atom located near the BF_2 group catalyzed the 1,2-BF_2 shift, resulting in the formation of a BODIHY product.[40] The rate of the shift in *trans*-**1** based on UV/Vis spectroscopy studies follows the order DMSO > DMF > DMAc, with a $\tau_{1/2}$ of 0.68 ± 0.03, 1.8 ± 0.2, and 3.3 ± 0.4 h, respectively (Table 2). The formation of BODIHY was confirmed using ^{1}H and ^{19}F NMR spectroscopies in DMSO-d_6 (Fig. S27). Specifically, the ^{19}F spectra showed the disappearance of the initial azo-BF_2 resonance signal at −145.0 ppm and the simultaneous appearance of a new signal at −123.5 ppm, which corresponds to the corresponding BODIHY dye.[40] The formation rate of BODIHY was determined to be 0.53 h, which aligns well with the result obtained from the UV/Vis measurements. In aprotic solvents with lower donor numbers, such as THF, acetone, and EA (Fig. S38–S40 and S48–S50), no 1,2-BF_2 is observed. Nonetheless, even though ultra-dry (H_2O < 50 ppm) solvents are used, the switches undergo slow solvent-assisted solvolysis (Fig. 3b). The reaction follows the order: THF > acetone > EA, with $\tau_{1/2}$ of, 44 ± 3, 53 ± 7, and 82 ± 15 h, respectively for *trans*-**1**. Similar trends are observed for *trans*-**2** (Table 2).

Finally, in alcohols methanol (MeOH), ethanol (EtOH), 1-propanol (*n*-PrOH), 2-propanol (*i*-PrOH), 2-methyl-1-propanol (*i*-BuOH), 2-butanol (*sec*-BuOH), and benzyl alcohol (BnOH, Fig. S28–S34 and S47) the switches quickly revert to their hydrazone precursors (Table 3 and Fig. 3c).[40]

To understand the different solvent-dependent outcomes, we correlated the reaction rates to various solvent parameters, including α, π^*, DN, acceptor number (AN), and the acidity, basicity, and polarity index (Z). In the case of *trans*-**1**, the best correlations for the 1,2-BF_2-shift rates were with the DN (R^2 = 0.95, Fig. 4a) and π^* (R^2 = 0.92, Fig. S51a).[44] Similarly, *trans*-**2** exhibited the best correlation with DN (R^2 = 0.91, Fig. 4b) followed by π^* (R^2 = 0.74, Fig. S51b). Other solvent parameters show much weaker correlations. These findings strongly suggest that the solvent donor number has the most substantial influence on the molecular reaction pathway in **1** and **2**. That is, solvents that donate lone pair electrons to the boron in the azo-BF_2 switches more readily result in faster 1,2-BF_2 shifts. As for the hydrolysis in alcohols, surprisingly, the process is not governed by the pK_a of the solvents, but rather by their hydrogen bond donating ability (α, Fig. 4c, R^2 = 0.97). Hydrogen bond donation ability is determined not solely by the intrinsic acidity (pK_a) of the solvent, but by a combination of factors, including the electronegativity of the hydrogen-bearing atom, the polarity of the hydrogen-donating bond, steric hindrance, and the overall solvent structure (including resonance effects). Under our experimental conditions, it appears that steric effects in protic solvents play a decisive role in modulating the reaction rate by influencing the accessibility and strength of hydrogen bonding at the coordination site. These findings highlight that the multifaceted nature of solvent interactions must be carefully considered when evaluating the stability of the N → B coordination bond in azo-BF_2 switches.

To elucidate the mechanism of the BF_2-shift and solvolysis reactions in *trans*-**1** and *trans*-**2**, we conducted DFT-based quantum chemical calculations in three representative solvents: dichloromethane (DCM, a weakly polar solvent), dimethyl sulfoxide (DMSO, a strong polar aprotic Lewis base), and methanol (MeOH, a protic solvent with moderate Lewis base strength). These calculations were performed at M06-2X/

Table 3 Summary of solvolysis data for *trans*-**1** in polar protic alcohols

Solvent	MeOH	EtOH	*n*-PrOH	*i*-PrOH	*i*-BuOH	*sec*-BuOH	BnOH
$\tau_{1/2}$[a] (h)	0.063 ± 0.005	0.13 ± 0.01	0.16 ± 0.01	0.38 ± 0.04	0.20 ± 0.01	0.42 ± 0.04	0.82 ± 0.09
k[b] (s^{-1})	$3.1 \pm 0.3 \times 10^{-3}$	$1.5 \pm 0.1 \times 10^{-3}$	$1.2 \pm 0.1 \times 10^{-3}$	$5.2 \pm 0.6 \times 10^{-4}$	$9.4 \pm 0.2 \times 10^{-4}$	$4.6 \pm 0.4 \times 10^{-4}$	$2.4 \pm 0.3 \times 10^{-4}$

[a] *Trans*-**1** decomposition half-life. [b] The reaction rate of decomposition.

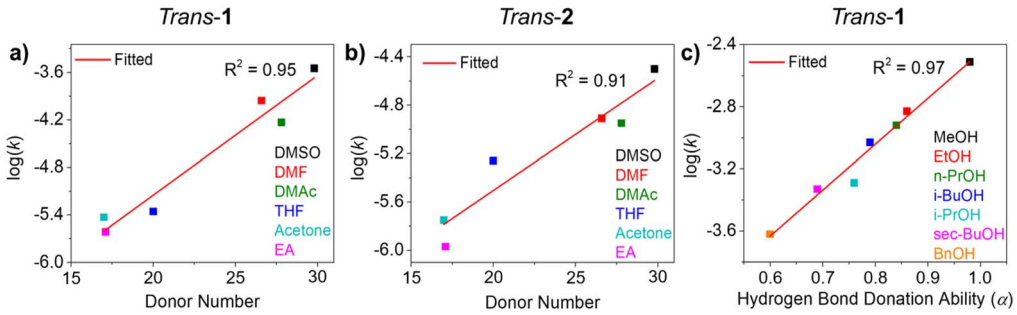

Fig. 4 Correlation of reaction rate with the most relevant parameter: (a) *trans*-**1** in aprotic solvents *versus* DN, (b) *trans*-**2** in aprotic solvents *versus* DN, and (c) *trans*-**1** in protic solvents *versus* α.

def2-TZVP/SMD level for single-point energies, with initial geometries optimized at the B3LYP-D3/def2-SVP/SMD level (for more computational details, please see the SI).

Starting with *trans*-**1** in DCM, the direct 1,2-BF_2 shift was found to have a high free energy activation barrier of 34.5 kcal-mol^{-1} through transition state **TS1a** (Fig. 5a). This substantial barrier suggests that the 1,2-BF_2 shift will unlikely proceed in

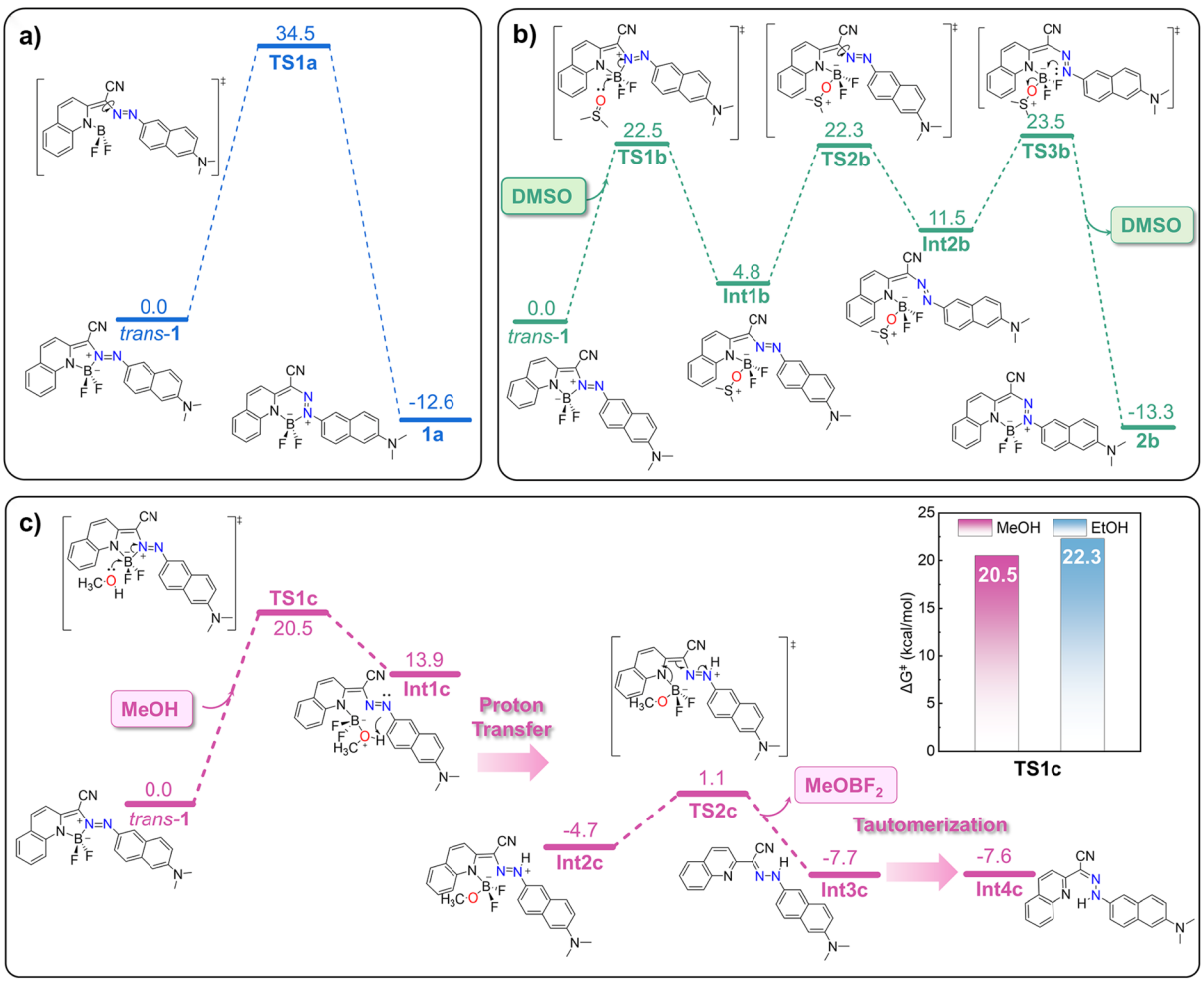

Fig. 5 Computed reaction mechanisms illustrating the 1,2-BF_2 shift in (a) DCM and (b) DMSO, as well as (c) the solvolysis of *trans*-**1** with MeOH. All calculations were performed at the M06-2X/def2-TZVP/SMD//B3LYP-D3/def2-SVP/SMD level of theory. The subpanel in (c) shows a comparison of the energy barriers at **TS1c** in methanol and ethanol. The free energy activation barriers ($\Delta G^{\ddagger}$) and free energy differences (ΔG^{0}) are relative to the individual starting species *trans*-**1**, and explicit solvent molecules are used when applicable. Values are free energies in kcal mol^{-1}. Panel (c) is not drawn to scale to improve clarity.

DCM, aligning with experimental observations. It is important to note that these calculations were performed using an implicit solvent model, as the 1,2-BF_2 shift in DCM is proposed to be a single-step process with no solvent mediation (Fig. S55).

The energy barrier for the 1,2-BF_2 shift reaction is significantly lower in DMSO than in DCM. Our modelling suggests that DMSO, a strong Lewis base with its high donor number, participates directly in the reaction, playing a critical role in the 1,2-BF_2 shift, *i.e.*, DMSO directly attacks the boron atom, displacing the azo group bound to it. Computations show that this substitution proceeds *via* transition state **TS1b**, requiring a free energy barrier of only 22.5 kcal mol^{-1} (Fig. 5b and S56), leading to intermediate **Int1b**, which is endergonic by 4.8 kcal mol^{-1}. Analysis of the structure of **Int1b** reveals a key bond distance of 2.91 Å for the broken B–N bond and 1.53 Å for the newly formed B–O bond, creating sufficient space for the rotation of the azo group, which occurs *via* the transition state **TS2b** ($\Delta G^{\ddagger}$ = 22.3 kcal mol^{-1}) resulting in intermediate **Int2b** (11.5 kcal mol^{-1}). Finally, dissociation of DMSO *via* **TS3b** ($\Delta G^{\ddagger}$ = 23.5 kcal mol^{-1}) and rebinding of the rotated azo group to the boron leads to the formation of the exergonic product **2b** (−13.3 kcal mol^{-1}). These calculated moderate energy barriers in DMSO explain why the 1,2-BF_2 shift occurs readily in this solvent, as observed experimentally.

The DFT calculations also indicate that in methanol, solvolysis is more facile than the 1,2-BF_2 shift (Fig. 5c and S57). Methanol, being a protic solvent, initiates the reaction by attacking the boron atom, leading to the displacement of the azo group *via* the transition state **TS1c** ($\Delta G^{\ddagger}$ = 20.5 kcal mol^{-1} relative to the free starting materials). This process is followed by a rearrangement through proton transfer (facilitated by surrounding solvent molecules) to **Int2c**. Subsequently, the dissociation of BF_2OMe occurs *via* **TS2c** ($\Delta G^{\ddagger}$ = 1.1 kcal mol^{-1}), resulting in the intermediate **Int3c** that tautomerizes to **Int4c**.[45]

The H-bonds between the two fluorine atoms in the BF_2 bridge and surrounding methanol molecules result in a lower azo group displacement energy barrier (20.5 kcal mol^{-1}) compared to DMSO (22.5 kcal mol^{-1}, Fig. 5b and c). Electrostatic potential energy surface analysis of *trans*-**1** derivatives reveals significant negative charge density at the fluorine atoms (Fig. S58 and Table S1). These H-bond interactions, partially accounted for in the solvent model, stabilize the transition states and lower the energy barriers. More importantly, the protic nature of methanol promotes solvolysis by donating a proton to *trans*-**1** and supports the formation of **Int2c** by enabling efficient proton diffusion. Notably, alcohol molecules act as H-bond donors, and their donating ability is a key factor governing the solvolysis rate of the azo-BF_2 compounds. When we modeled a similar solvolysis reaction in ethanol (α = 0.86), which has a weaker H-bond donating ability than methanol (α = 0.98), the energy barrier of **TS1** increased from 20.5 to 22.3 kcal mol^{-1} (Fig. 5c and Table S2), respectively. These findings demonstrate that the H-bond donating ability of the protic solvent significantly influences reaction kinetics, which is consistent with experimental observations. It is also worth mentioning that methanol is more effective than ethanol at facilitating proton transfer, owing to its greater polarity and smaller steric hindrance. These properties enhance the formation of **Int2c** and promote more efficient solvolysis. The calculated results for *trans*-**2** showed similar trends (Fig. S59–S64).

Conclusions

In summary, the synthesis and characterization of two structurally distinct azo-BF_2 photoswitches presented in this work underscore the significant potential of structural modulation in enhancing their photophysical performance. We demonstrate that expanding the π-conjugation profoundly influences the activation wavelength and photoswitching performance, with switch **1** achieving an extended NIR absorption profile, and switch **2** benefiting from improved separation of the absorption bands. The solvent-dependent behavior, particularly the 1,2-BF_2 shift, highlights the critical role of solvent donor number in dictating reaction pathways and product stability. On the other hand, the observed solvent-mediated solvolysis showcases the importance of the solvent's hydrogen bond donation ability in driving the process. Importantly, the interplay between solvent proticity and steric effects can be leveraged to mitigate the reaction. Moreover, the data indicate that lowering accessibility to the N → B bond through steric hindrance can lower its reactivity. Overall, the gained insights can be harnessed to further the design of these efficient visible and NIR-responsive photoswitches, and expand opportunities in adaptive materials, molecular devices, and energy storage applications.

Author contributions

Q. Qi conceived the initial project, synthesized the compounds, and conducted their photophysical and structural characterization. Q. Qi also wrote the original draft of the manuscript. H. Fu investigated and analyzed the solvent-dependent behavior of the compounds and co-wrote the original draft. L. Peng performed and summarized the DFT calculations under the guidance of X. Liu. S. P. assisted with UV-Vis absorption measurements. I. A. supervised the overall project and provided critical revisions to the manuscript.

Conflicts of interest

There are no conflicts to declare.

Data availability

All data are available in the main text and the SI. See DOI: https://doi.org/10.1039/d5sc05042a.

Acknowledgements

X. L. thank the Ministry of Education, Singapore (MOE-T2EP10222-0001), for financial support. The authors are also grateful for the computational resources provided by the Singapore University of Technology and Design (SUTD) and the National Supercomputing Centre, Singapore. Q. Q. acknowledges Jiangsu Specially Appointed Professorship.

References

1 W. A. Velema, W. Szymanski and B. L. Feringa, *J. Am. Chem. Soc.*, 2014, **136**, 2178.
2 D. Bléger and S. Hecht, *Angew. Chem., Int. Ed.*, 2015, **54**, 11338.
3 M. M. Lerch, M. J. Hansen, G. M. van Dam, W. Szymanski and B. L. Feringa, *Angew. Chem., Int. Ed.*, 2016, **55**, 10978.
4 M. Wegener, M. J. Hansen, A. J. M. Driessen, W. Szymanski and B. L. Feringa, *J. Am. Chem. Soc.*, 2017, **139**, 17979.
5 K. Hüll, J. Morstein and D. Trauner, *Chem. Rev.*, 2018, **118**, 10710.
6 I. M. Welleman, M. W. H. Hoorens, B. L. Feringa, H. H. Boersma and W. Szymański, *Chem. Sci.*, 2020, **11**, 11672.
7 H. Wang, H. K. Bisoyi, X. Zhang, F. Hassan and Q. Li, *Chem.–Eur. J.*, 2022, **28**, e202103906.
8 Y. Xu, Y. Tang and Q. Li, *Adv. Funct. Mater.*, 2024, 2416359.
9 R. Siewertsen, H. Neumann, B. Buchheim-Stehn, R. Herges, C. Näther, F. Renth and F. Temps, *J. Am. Chem. Soc.*, 2009, **131**, 15594.
10 A. A. Beharry, O. Sadovski and G. A. Woolley, *J. Am. Chem. Soc.*, 2011, **133**, 19684.
11 H. M. D. Bandara and S. C. Burdette, *Chem. Soc. Rev.*, 2012, **41**, 1809.
12 D. Bléger, J. Schwarz, A. M. Brouwer and S. Hecht, *J. Am. Chem. Soc.*, 2012, **134**, 20597–20600.
13 S. Samanta, A. A. Beharry, O. Sadovski, T. M. McCormick, A. Babalhavaeji, V. Tropepe and G. A. Woolley, *J. Am. Chem. Soc.*, 2013, **135**, 9777.
14 M. Dong, A. Babalhavaeji, S. Samanta, A. A. Beharry and G. A. Woolley, *Acc. Chem. Res.*, 2015, **48**, 2662.
15 M. Hammerich, C. Schütt, C. Stähler, P. Lentes, F. Röhricht, R. Höppner and R. Herges, *J. Am. Chem. Soc.*, 2016, **138**, 13111.
16 P. Lentes, E. Stadler, F. Röhricht, A. Brahms, J. Gröbner, F. D. Sönnichsen, G. Gescheidt and R. Herges, *J. Am. Chem. Soc.*, 2019, **141**, 13592.
17 L. N. Lameijer, S. Budzak, N. A. Simeth, M. J. Hansen, B. L. Feringa, D. Jacquemin and W. Szymanski, *Angew. Chem., Int. Ed.*, 2020, **59**, 21663.
18 T. Fukaminato, T. Hirose, T. Doi, M. Hazama, K. Matsuda and M. Irie, *J. Am. Chem. Soc.*, 2014, **136**, 17145.
19 N. M.-W. Wu, M. Ng, W. H. Lam, H.-L. Wong and V. W.-W. Yam, *J. Am. Chem. Soc.*, 2017, **139**, 15142.
20 H. Xi, Z. Zhang, W. Zhang, M. Li, C. Lian, Q. Luo, H. Tian and W.-H. Zhu, *J. Am. Chem. Soc.*, 2019, **141**, 18467.
21 Z. Zhang, W. Wang, P. Jin, J. Xue, L. Sun, J. Huang, J. Zhang and H. Tian, *Nat. Commun.*, 2019, **10**, 4232.
22 S. Wiedbrauk and H. Dube, *Tetrahedron Lett.*, 2015, **56**, 4266.
23 C.-Y. Huang, A. Bonasera, L. Hristov, Y. Garmshausen, B. M. Schmidt, D. Jacquemin and S. Hecht, *J. Am. Chem. Soc.*, 2017, **139**, 15205.
24 L. Köttner, E. Ciekalski and H. Dube, *Angew. Chem., Int. Ed.*, 2023, **62**, e202312955.
25 M. Zitzmann, M. Fröhling and H. Dube, *Angew. Chem., Int. Ed.*, 2024, **63**, e202318767.
26 M. Jacquet, L. M. Uriarte, F. Lafolet, M. Boggio-Pasqua, M. Sliwa, F. Loiseau, E. Saint-Aman, S. Cobo and G. Royal, *J. Phys. Chem. Lett.*, 2020, **11**, 2682.
27 K. Klaue, W. Han, P. Liesfeld, F. Berger, Y. Garmshausen and S. Hecht, *J. Am. Chem. Soc.*, 2020, **142**, 11857.
28 S. Helmy, F. A. Leibfarth, S. Oh, J. E. Poelma, C. J. Hawker and J. Read de Alaniz, *J. Am. Chem. Soc.*, 2014, **136**, 8169.
29 M. M. Lerch, W. Szymański and B. L. Feringa, *Chem. Soc. Rev.*, 2018, **47**, 1910.
30 R. Castagna, G. Maleeva, D. Pirovano, C. Matera and P. Gorostiza, *J. Am. Chem. Soc.*, 2022, **144**, 15595.
31 M. Clerc, S. Sandlass, O. Rifaie-Graham, J. A. Peterson, N. Bruns, J. R. de Alaniz and L. F. Boesel, *Chem. Soc. Rev.*, 2023, **52**, 8245.
32 C. A. Reyes, A. Karr, C. A. Ramsperger, A. T. G. K, H. J. Lee and E. Picazo, *J. Am. Chem. Soc.*, 2025, **147**, 10.
33 S. Crespi, N. A. Simeth and B. König, *Nat. Rev. Chem.*, 2019, **3**, 133.
34 T. Dang, Z.-Y. Zhang and T. Li, *J. Am. Chem. Soc.*, 2024, **146**, 19609.
35 Y. Yang, R. P. Hughes and I. Aprahamian, *J. Am. Chem. Soc.*, 2012, **134**, 15221.
36 Y. Yang, R. P. Hughes and I. Aprahamian, *J. Am. Chem. Soc.*, 2014, **136**, 13190.
37 Q. Qi, J. T. Plank, A. R. Lippert and I. Aprahamian, *Chem*, 2024, **10**, 3575.
38 Q. Qiu, Q. Qi, J. Usuba, K. Lee, I. Aprahamian and G. G. D. Han, *Chem. Sci.*, 2023, **14**, 11359.
39 H. Qian, Y.-Y. Wang, D.-S. Guo and I. Aprahamian, *J. Am. Chem. Soc.*, 2017, **139**, 1037.
40 Q. Qi, S. Huang, X. Liu and I. Aprahamian, *J. Am. Chem. Soc.*, 2024, **146**, 6471.
41 Y. Marcus, *Chem. Soc. Rev.*, 1993, **22**, 409.
42 C. Y. Huang, A. Bonasera, L. Hristov, Y. Garmshausen, B. M. Schmidt, D. Jacquemin and S. Hecht, *J. Am. Chem. Soc.*, 2017, **139**, 15205.
43 B. Shao, H. Qian, Q. Li and I. Aprahamian, *J. Am. Chem. Soc.*, 2019, **141**, 8364.
44 Acetone, EA, and THF were included in the DN correlation analysis even though they do not induce an observable BF_2 shift. We hypothesize that the rate determining step in both reactions is the solvent attack on the boron center, and so we are using the hydrolysis rate in these solvents as place holders for the fastest rate at which such a shift can take place.
45 S. M. Landge, E. Tkatchouk, D. Benítez, D. A. Lanfranchi, M. Elhabiri, W. A. Goddard and I. Aprahamian, *J. Am. Chem. Soc.*, 2011, **133**, 9812.